

Cramer-Rao Bounds for Target Parameter Estimation in a Bi-Static IRS-Assisted Radar Configuration

Sanjeeva Reddy S, *Graduate Student Member, IEEE*, Vinod Veera Reddy, *Member, IEEE*

Abstract—Non-Line-of-Sight (NLoS) sensing and detection of low-observable (stealth) targets are challenging for conventional radar due to blockage and severe propagation loss. Intelligent Reflective Surface (IRS)-assisted radar can extend the field-of-view (FOV), but common architectures rely on the four-hop radar-IRS-target-IRS-radar link, whose attenuation limits estimation performance. This paper proposes an alternative architecture, that exploits the target-scattered component received at a spatially separated IRS and redirected back to a mono-static radar receiver. The geometry provides bi-static/multi-static-like diversity using a passive panel, while retaining a mono-static front-end and avoiding inter-node time synchronization concerns. We develop a signal model for the proposed configuration and recast it into a compact, parameterized form that is suitable for angle estimation. Using this reformulation, we derive the Fisher Information Matrix and the associated Cramér–Rao Lower Bounds (CRLB) for target azimuth and elevation angles with respect to the IRS. Numerical evaluations quantify the impact of various signal-model parameters on the achievable bounds. These results provide insights on the parameter-estimation limits within the FOV against SNR, snapshots and IRS elements.

Index Terms—Cramer-Rao Bounds (CRB), bi-static, multi-static, IRS-assisted radar.

I. INTRODUCTION

Radar has historically been a vital sensing technology capable of *active* and *passive* detection, target tracking, high-res imaging, and increasingly, sensing in *Non-Line-of-Sight* (NLoS) environments [1], [2], [3], [4]. Conventional mono-static radars usually perform well when targets are within their Line-of-Sight (LoS), enabling precise measurement of range, Doppler shifts, and directions. However, when obstacles block the LoS, the effectiveness of traditional radar diminishes significantly or results in complete detection failure, driving the innovation of new NLoS sensing architectures.

A common method for enabling NLoS radar sensing involves using an *Intelligent Reflective Surface* (IRS). An IRS is made up of passive, adaptable reflecting elements that can steer incident electromagnetic waves, creating controllable pathways beyond the LoS when positioned appropriately. This *IRS-assisted radar* technology can be well suited in defence, automotive sensing, and modern wireless systems to expand the field-of-view (FOV) and improve NLoS target detection capabilities [5], [6], [7]. Meanwhile, the presence of an IRS introduces multiple possible signal paths from the

target to the radar. Specifically, deploying an IRS results in four key propagation paths (which vary based on geometry and blockage), that include:

- (P1) Radar \rightarrow Target \rightarrow Radar,
- (P2) Radar \rightarrow IRS \rightarrow Target \rightarrow IRS \rightarrow Radar,
- (P3) Radar \rightarrow Target \rightarrow IRS \rightarrow Radar,
- (P4) Radar \rightarrow IRS \rightarrow Target \rightarrow Radar.

Most IRS-assisted radar studies typically focus on the dominant LoS component (P1) and the IRS-enabled NLoS component (P2) [8]. NLoS sensing via (P2) has been widely studied, including the derivation of Cramér–Rao Lower Bounds (CRLB) for selected target parameters [9]. However, while IRS phase weights can provide beamforming gain, they cannot fundamentally mitigate the severe path loss inherent to the four-hop channel in (P2), due to compounded attenuation over the radar-IRS and IRS-target links [10].

To mitigate performance degradation due to path loss and scattering from stealth targets, radar system design has also inclined towards bi-static and multi-static configurations. Unlike mono-static radar, in which the transmitter (Tx) and receiver (Rx) are co-located, bi-static and multi-static radars spatially separate the Tx and Rx(s), thereby forming a distributed sensing architecture [11], [12], [13]. This separation enables the receiver to observe the target from a viewpoint that is not constrained by the LoS path between the transmitter and target. In multi-static reception, multiple spatially separated receivers observe the target returns, which can improve detection probability and tracking performance through spatial diversity [14], [15]. Such configurations are particularly useful for detecting low-observable (stealth) targets and for sensing space objects, making them attractive for modern defence and space applications [16], [17]. Despite these advantages, they introduce important practical limitations, most notably stringent time and phase synchronization requirements between the Tx and distributed Rx (s), along with increased hardware cost and maintenance overhead compared to mono-static radar.

Upon investigating these trade-offs, we observe the need for a configuration that (i) reduces the effective path loss relative to the double-IRS (P2) route, and (ii) avoids inter-node time synchronization errors inherent in bi-static/multi-static radars. In this work, we focus on the *third path* (P3), i.e., **Radar \rightarrow Target \rightarrow IRS \rightarrow Radar**, which is often overlooked but is extremely useful. As will be shown, this path is analogous to

Sanjeeva Reddy S and Vinod Veera Reddy are affiliated with Dept. of Electronics and Communication Engineering, International Institute of Information Technology Bangalore (IIITB), Bengaluru, India, 560100. e-mail: sanjeevareddy.s414@ieec.org and vinod.reddy@iiitb.ac.in

a bi-static/multi-static observation geometry because the IRS provides a spatially displaced “listening” viewpoint relative to the radar, yet it remains a passive structure. This motivates a bi-static-like configuration based on IRS-assisted radar. A similar configuration is presented in [18] for stealth target detection. However, parameter estimation in such a scenario is not discussed.

In the proposed IRS-assisted Radar configuration from [18], an IRS is positioned spatially away from the mono-static radar. The radar transmits a signal into its FOV; the target reflects and scatters the incident energy. The IRS is oriented (and configured) to “look” toward a specific direction that intersects the radar’s FOV at a different angle, receive the scattered signal from the target, and steer it back to the radar receiver. In this manner, the sensing chain leverages (P3), mimicking certain advantages of bi-static/multi-static radar while maintaining a mono-static radar front-end, thereby eliminating explicit time synchronization errors between Tx and Rx. Moreover, employing an IRS panel to realize a bi-static-like sensing geometry in challenging scenarios (e.g., stealth target detection) introduces a novel paradigm: from a geometric sensing standpoint, the IRS-assisted propagation path can often be interpreted as effectively *translating the sensing aperture* to the IRS location and subsequently mapping the estimated target coordinates back into the original radar reference frame.

The contributions of the paper are summarized as follows:

- The IRS-assisted radar configuration is presented in comparison to bi-static/multi-static radar and existing IRS-assisted radars. The associated signal model is systematically developed and reformulated into a parameterized model suitable for CRB/CRLB derivation.
- We derive Cramér–Rao bounds (CRB) for the target angle parameters (azimuth and elevation) under the proposed signal model.
- Extensive simulation studies are performed to validate the performance of the radar system under different geometric and channel conditions.

The paper is organized as follows: Section II explains in detail the proposed radar configuration. Section III provides the detailed mathematical derivation of the signal model and the target parameters. Based on these target parameters, the theoretical CRB limits are derived in Section IV. Section V discusses the numerical results in relation to the theoretical bounds, and Section VI concludes the paper.

II. IRS-ASSISTED RADAR SETUP

Bi-static radar separates the transmitter and receiver, forming a triangle with the target, unlike mono-static radar’s single-axis setup. This concept generalizes to multi-static radar, which uses multiple spatially dispersed transmitters and receivers to gain spatial diversity. Multi-static systems observe targets from several angles, enhancing the detection of complex or stealthy targets whose Radar Cross Section (RCS) varies with aspect. However, effectively exploiting these advantages requires careful spatial arrangement of the receivers, as discussed in [19].

The IRS-assisted radar setup replaces traditional bi-/multi-static receiver nodes with low-cost IRS panels that reflect scattered signals toward nearby radar sensors [18]. By carefully designing the IRS element weights, the system achieves sufficient beamforming gain to offset longer propagation paths. Fixed IRS placement simplifies radar-IRS channel estimation, while the large number of IRS elements enhances parameter estimation and mitigates synchronization issues typical in conventional bi-/multi-static radars, which rely on fewer, more expensive antennas.

The text introduces an “IRS-static radar” configuration, based on the IRS-assisted radar setup in [20], that uses only two relevant paths: the monostatic radar path and the Radar \rightarrow Target \rightarrow IRS \rightarrow Radar path, with the latter being crucial for stealth targets. Unlike prior IRS-assisted radar work [21], which places the IRS near the radar or target to boost signal strength and relies on a 4-path model (Radar \rightarrow IRS \rightarrow Target \rightarrow IRS \rightarrow Radar)[cite 4 path model papers], the proposed design positions the IRS panel away from the radar and operates it in simplex mode so that energy always flows Target \rightarrow IRS \rightarrow Radar. This yields a simpler IRS (lower design and circuitry complexity), forms an effective 3-path model (Radar \rightarrow Target \rightarrow IRS \rightarrow Radar), reduces path loss compared to conventional 4-path IRS-assisted systems, and functionally emulates a bi-static radar configuration, hence the term “IRS-static radar.”

III. SIGNAL MODEL

Consider an air-target scenario with K targets defined with respect to the radar coordinate system, with the radar located at $\mathbf{r}_R = [0, 0, 0]^T$. Let the k th target parameters—namely position, velocity, azimuth angle, and elevation angle—be given by $\mathbf{r}_k = [x_k, y_k, z_k]^T$, $\mathbf{v}_k = [v_{kx}, v_{ky}, v_{kz}]^T$, $\theta_k^{(az)}$, and $\theta_k^{(el)}$, respectively. Without loss of generality, we consider a single IRS panel with $L_h \times L_v$ reflecting elements located at \mathbf{r}_I in the radar coordinate system. Let the k th target subtend azimuth and elevation angles $\psi_k^{(az)}$ and $\psi_k^{(el)}$, respectively, as seen from the IRS coordinate system, as illustrated in Fig. 1b. We assume a phased-array radar with $M_T = M_R$ transceivers co-located at \mathbf{r}_R .

When the beamformed transmit signal $\mathbf{s}(t) \in \mathbb{C}^{M_T \times 1}$ interacts with the k th target, we focus on two scattered components of interest: (i) the monostatic return, and (ii) the component that propagates toward the IRS panel. Denoting the channel between the radar and the k th target by $\mathbf{g}_k \in \mathbb{C}^{1 \times M_T}$, the monostatic (ms) component can be expressed as

$$\mathbf{y}^{\text{ms}}(t, t_l) = \sum_{k=1}^K \alpha_k^{\text{ms}} \mathbf{g}_k \mathbf{g}_k^H \mathbf{s}(t - \tau'_{k,l}), \quad (1)$$

where H denotes the conjugate transpose and the channel \mathbf{g}_k is assumed reciprocal. Here, α_k^{ms} denotes the monostatic target response strength, t and t_l represent the fast-time and slow-time variables, respectively, and $\tau'_{k,l} = 2(\|\mathbf{r}_k - \mathbf{r}_R\|_2)/c$ is the two-way path delay between the radar and the k th target located at \mathbf{r}_k .

Next, we define the line-of-sight (LoS) channel between the k th target and the IRS panel as $\mathbf{h}_k \in \mathbb{C}^{L_h L_v \times 1}$, and

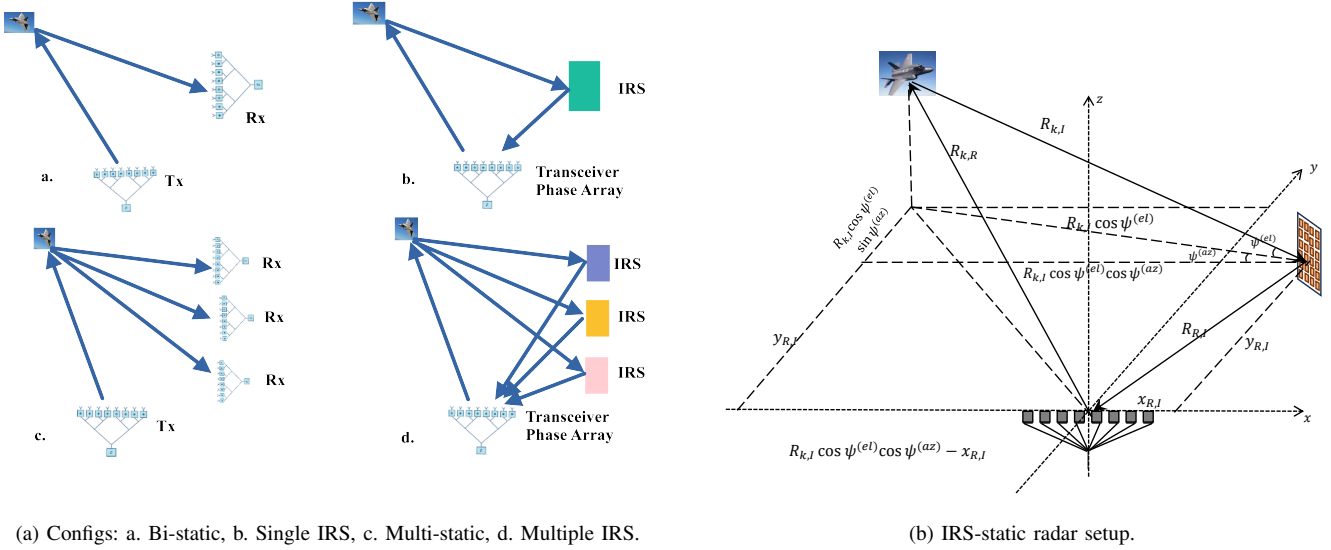


Fig. 1: Comparison of radar configurations (Left) and the IRS-static radar setup (Right).

the channel between the IRS panel and the phased-array transceiver as $\mathbf{F} \in \mathbb{C}^{M_R \times L}$. For a 2-D IRS panel, $L = L_h L_v$, where L_h and L_v denote the number of elements along the horizontal and vertical dimensions, respectively. The signal received at the radar via the IRS path (denoted as “is”) is given by

$$\mathbf{y}^{\text{is}}(t, t_l) = \sum_{k=1}^K \alpha_k^{\text{is}} \mathbf{F} \mathbf{D} \mathbf{h}_k \mathbf{g}_k^H \mathbf{s}(t - \tau_{k,l}), \quad (2)$$

where α_k^{is} is the target response strength through the IRS path and $\mathbf{D} = \text{diag}(d_1, \dots, d_l, \dots, d_{L_h L_v}) \in \mathbb{C}^{L_h L_v \times L_h L_v}$, such that $d_l = \zeta_l e^{-l\rho_l}$, such that $|\zeta_l| = 1$ and ρ_l represents the phase shift induced by the l -th reflecting element of the IRS $\forall 1 \leq l \leq L_h L_v$. It is important to note that the total path delay $\tau_{k,l} > \tau_{k,l}^{\text{ms}}$, and is given by

$$\tau_{k,l} = \frac{\|\mathbf{r}_k - \mathbf{r}_R\|_2 + \|\mathbf{r}_k - \mathbf{r}_I\|_2 + \|\mathbf{r}_I - \mathbf{r}_R\|_2}{c}. \quad (3)$$

Accordingly, the overall received signal at the transceiver can be written as

$$\mathbf{y}(t, t_l) = \mathbf{y}^{\text{ms}}(t, t_l) + \mathbf{y}^{\text{is}}(t, t_l) + \mathbf{v}(t, t_l), \quad (4)$$

where $\mathbf{v}(t, t_l)$ is an additive white Gaussian noise (AWGN) vector. For conventional targets, α_k^{ms} is typically large; hence, returns from both paths must, in principle, be processed. However, since the monostatic and IRS-assisted paths incur different delays, the corresponding contributions can be separated and processed independently. This separation can be achieved via beam-space processing. Because the direction (and hence the spatial signature) of the IRS relative to the phased-array radar is known, we construct M receive beams steered toward the IRS with some degree of overlap. The

beam-space output sampled at fast-time interval T_s is then given by

$$\begin{aligned} \bar{\mathbf{y}}(nT_s, t_l) &= \mathbf{W} \{ \mathbf{y}^{\text{ms}}(nT_s, t_l) + \mathbf{y}^{\text{is}}(t, t_l) + \mathbf{v}(t, t_l) \} \\ &\approx \sum_{k=1}^K \alpha_k^{\text{is}} \bar{\mathbf{F}} \mathbf{D} \mathbf{h}_k \mathbf{g}_k^H \mathbf{s}(nT_s - \tau_{k,l}) + \bar{\mathbf{v}}(nT_s, t_l), \end{aligned} \quad (5)$$

where $\bar{\mathbf{F}} = \mathbf{W} \mathbf{F}$ and $\mathbf{W} \in \mathbb{C}^{M \times M_R}$ is the beam-space matrix whose beamforming vectors preserve (primarily) the signal arriving from the IRS direction. We assume that the monostatic component is sufficiently suppressed by these IRS-pointing beams.

Since parameter extraction from conventional targets using the monostatic path is well studied, we focus in this paper on target parameter estimation using the IRS-path signal in (5). The radar data cube $\mathbf{Y} \in \mathbb{C}^{M \times N \times L}$, where N and L denote the numbers of fast-time and slow-time samples, respectively, is processed via a discrete Fourier transform (DFT) along the slow-time dimension to obtain M Range-Doppler (RD) maps, $\mathbf{Y}_{\text{RD}} = \mathcal{F}_L \{ \mathbf{Y} \}$, where $\mathcal{F}_L \{ \cdot \}$ is an L -point DFT operator. Due to the superposition of the K target responses, $\mathbf{Y}_{\text{RD}} = \sum_{k=1}^K \mathbf{Y}_{\text{RD}}^k$, where \mathbf{Y}_{RD}^k denotes the RD contribution due to the k th target alone. A constant false-alarm-rate (CFAR) [19] detector (or its variants) provides $K_P \leq K$ RD bins corresponding to true detections; some bins may contain multiple targets. Therefore, $K = \sum_{p=1}^{K_P} P_k$, where P_k denotes the number of targets present in the k th detected RD bin, (\hat{R}_k, \hat{v}_k) . Note that $\hat{R}_k = \frac{c\tau_{k,l}|_{l=0}}{2}$ corresponds to the round-trip distance via the IRS, while \hat{v}_k denotes the relative velocity of the target with respect to the radar.

The observation vector for the k th RD bin across the M beams is given by

$$\bar{\mathbf{y}}_k = \bar{\mathbf{F}} \mathbf{D} \sum_{p=1}^{P_k} \mathbf{h}_p \mathbf{g}_p^H \mathbf{s} + \bar{\mathbf{v}}_k, \quad (6)$$

We denote the channel between the radar and the p th target as $\mathbf{g}_p = \alpha_p^{(g)} \mathbf{a}_{M_T}(\theta_p^{(az)}, \theta_p^{(el)})$, where $\mathbf{a}_{M_T}(\theta_p^{(az)}, \theta_p^{(el)})$ is the steering vector toward the target as seen from the transmit array. Similarly, we write $\mathbf{h}_p = \alpha_p^{(h)} \mathbf{a}_{L_h L_v}(\psi_p^{(az)}, \psi_p^{(el)})$, where $\mathbf{a}_{L_h L_v}(\psi_p^{(az)}, \psi_p^{(el)}) = \mathbf{a}_{L_v}(\psi_p^{(az)}) \otimes \mathbf{a}_{L_h}(\psi_p^{(el)})$ is the steering vector toward the target as observed from the IRS panel, and \otimes denotes the Kronecker product. Defining $\alpha_p = \alpha_p^{(h)} \alpha_p^{(g)}$, (6) can be rewritten as

$$\bar{\mathbf{y}}_k = \bar{\mathbf{F}}\mathbf{D} \sum_{p=1}^{P_k} \alpha_p \mathbf{a}_{L_h L_v}(\psi_p^{(az)}, \psi_p^{(el)}) \times \mathbf{a}_{M_T}(\theta_p^{(az)}, \theta_p^{(el)})^H \mathbf{s} + \bar{\mathbf{v}}_k. \quad (7)$$

With \hat{R}_k and \hat{v}_k obtained from the constant false-alarm-rate (CFAR) detector, the parameters $\theta_k^{(az)}, \theta_k^{(el)}, \psi_k^{(az)}, \psi_k^{(el)}, \forall k \in [1, K]$ are to be estimated. Importantly, the 3-D target position can be determined using only a subset of these parameters. Let $R_{k,R}$ and $R_{k,I}$ denote the distances from the k th target to the radar and to the IRS, respectively. Then the estimated range inferred from the path delay satisfies

$$\hat{R}_k = R_{k,R} + R_{k,I} + R_{I,R}, \quad (8)$$

where the IRS–radar distance $R_{I,R}$ is assumed known.

It follows that estimating $\psi_k^{(az)}$ and $\psi_k^{(el)}$, together with $R_{k,I}$, yields the k th target position $\mathbf{r}'_k = [x'_k, y'_k, z'_k]$ with respect to the IRS coordinate system. The target position in the radar coordinate system can then be obtained via

$$\mathbf{r}_k = \mathbf{r}'_k + \mathbf{r}_I. \quad (9)$$

Alternatively, the target position can be obtained directly by estimating $\theta_k^{(az)}$ and $\theta_k^{(el)}$ along with $R_{k,R}$ from \hat{R}_k . In the next section, we present a technique to estimate the target position with respect to the IRS.

A. Design of IRS Weights

To achieve performance analogous to a bi-static/multi-static radar, the IRS-static radar must incorporate the effective field-of-view (FOV) of the corresponding distributed configuration into its design. Consider a bi-static radar as illustrated in Fig. 2(a), where the intersection of the transmit and receive beams defines the FOV for target detection. In the equivalent IRS-static radar depicted in Fig. 2(b), the bi-static receiver is replaced by the IRS panel. The IRS weights are then designed to redirect the incoming signal toward the radar, which hosts both the transmitter and the receive array.

To realize the desired FOV, the bi-static radar receiver would be oriented toward the direction $(\psi_0^{(az)}, \psi_0^{(el)})$. For the IRS-static radar, the IRS weights must be configured such that signals received from this angular region are redirected toward the radar receiver, which is located at an angle $(\psi_R^{(az)}, \psi_R^{(el)})$ relative to the IRS panel. The IRS weight design primarily aims to compensate for the relative phase across the reflecting elements along the overall propagation path. Defining the diagonal matrices $\mathbf{A}_0 = \text{diag}\{\mathbf{a}(\psi_0^{(az)}, \psi_0^{(el)})\}$

and $\mathbf{A}_R = \text{diag}\{\mathbf{a}(\psi_R^{(az)}, \psi_R^{(el)})\}$, the diagonal IRS weight matrix \mathbf{D} should satisfy

$$\mathbf{A}_0 \mathbf{D} \mathbf{A}_R = \mathbf{I}, \quad (10)$$

where \mathbf{I} is the identity matrix. The resulting solution is

$$\mathbf{D} = \mathbf{A}_0^* \mathbf{A}_R^*. \quad (11)$$

For targets in the vicinity of $(\psi_0^{(az)}, \psi_0^{(el)})$, the IRS panel redirects the response back to the radar. The maximum beamforming gain from the IRS is achieved when the target is located exactly in the direction $(\psi_0^{(az)}, \psi_0^{(el)})$. The performance of this IRS weight design is analyzed in the simulation results section.

B. Recasting the signal model for Target Parameter Estimation

It is evident from (7) that the received signal corresponds to a point in 3-D space defined by the intersection of $\mathbf{a}_{L_v L_h}(\psi_p^{(az)}, \psi_p^{(el)})$ and $\mathbf{a}_{M_T}(\theta_p^{(az)})$, further constrained by the round-trip delay. From (7), we combine the total gain (α_p) and the transmitter steering vector (\mathbf{a}_{M_T}) with the beamformed transmit signal (\mathbf{s}) so as to enable estimation of the angle information with respect to the IRS. The resulting compact representation is

$$\bar{\mathbf{y}}_k = \bar{\mathbf{F}}\mathbf{D}\mathbf{A}\bar{\mathbf{x}} + \bar{\mathbf{v}}_k, \quad (12)$$

where $\bar{\mathbf{x}} = \sum_{p=1}^{P_k} \alpha_p \mathbf{a}_{M_T}(\theta_p^{(az)}, \theta_p^{(el)}) \mathbf{s}$ and the dictionary matrix $\mathbf{A} \in \mathbb{C}^{L_h L_v \times G_R}$ corresponds to the AoA space around the IRS such that

$$\mathbf{A} = [\mathbf{a}(\psi_1), \dots, \mathbf{a}(\psi_{G_R})]. \quad (13)$$

The grid points (ψ_{G_R}) are expressed as $\Psi = \{\psi_z : \psi_z = (\psi_z^{(az)}, \psi_z^{(el)}), \psi_z^{(az)} \in [-\pi/2, \pi/2], \psi_z^{(el)} \in [0, \pi/2], 1 \leq z \leq G_R\}$. Based on the target field of view with respect to the IRS, the angular region (and hence the number of grid points) can be reduced. In the following section, Cramer-Rao Bounds are derived for the signal model presented above.

IV. CRAMER RAO BOUNDS

We identify the target parameters from the proposed signal model (12) as

$$\zeta = [\psi^{az}, \psi^{el}]^T, \quad (14)$$

where $\psi^{az} = [\psi_1^{az}, \psi_2^{az}, \dots, \psi_k^{az}]$ and $\psi^{el} = [\psi_1^{el}, \psi_2^{el}, \dots, \psi_k^{el}]$ denote the true azimuth and elevation angles, respectively, for k targets, resulting in $\zeta \in \mathbb{R}^{2k \times 1}$. Our objective is to characterize the fundamental error bound, i.e., the minimum achievable variance, for estimating these angle parameters under the proposed k -target signal model using the Cramér–Rao Lower Bound (CRLB) framework.

Several approaches exist for deriving Cramér–Rao bounds depending on the assumptions and structure of the signal model [22]. For IRS-assisted radar with a beamformed transmit signal (\mathbf{s}) treated as an unknown waveform, a corresponding CRB derivation is provided in [8]. In our setting, we assume the signal waveform to be deterministic and the test statistics to be known. Accordingly, we adopt the CRB

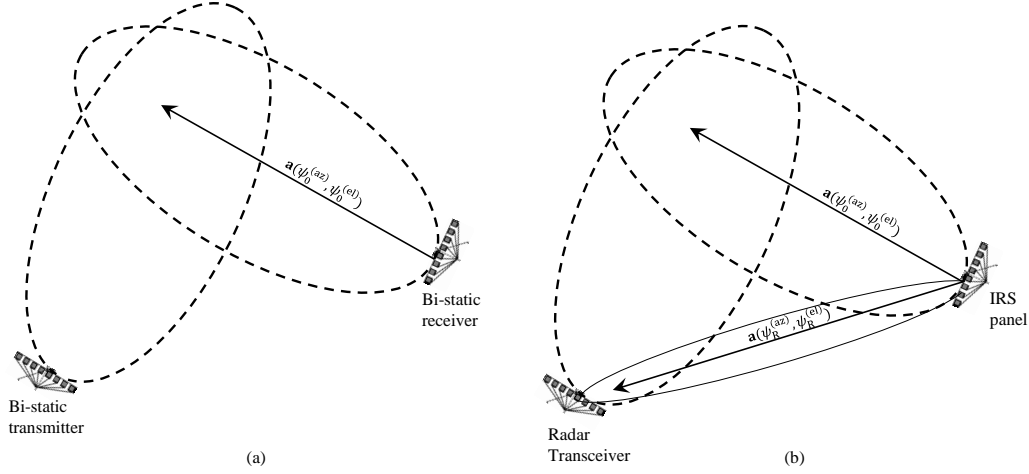


Fig. 2: Field-of-view for (a) Bi-static radar, (b) IRS-static radar.

formulation for known deterministic waveforms for planar arrays presented in [22] in order to obtain the angle-estimation error bounds associated with the IRS observations.

For CRLB analysis, the proposed signal model in (12) is rearranged as

$$\mathbf{y}(k) = \bar{\mathbf{A}}\bar{\mathbf{x}}(k) + \bar{\mathbf{v}}, \quad (15)$$

where $\bar{\mathbf{A}} = \bar{\mathbf{F}}\mathbf{D}\mathbf{A}(\psi^{az}, \psi^{el})$. This compact representation reduces notational complexity by capturing the signal structure across snapshots within a single matrix form.

The Fisher Information Matrix (FIM) associated with the above signal model and the parameter vector of interest is given by

$$\mathbf{J} = \begin{bmatrix} \mathbf{J}_{\psi^{az}, \psi^{az}} & \mathbf{J}_{\psi^{az}, \psi^{el}} \\ \mathbf{J}_{\psi^{el}, \psi^{az}} & \mathbf{J}_{\psi^{el}, \psi^{el}} \end{bmatrix} \quad (16)$$

The vector derivative of the steering vector $\bar{\mathbf{A}}$ is defined as

$$\mathbf{z}_i = \begin{bmatrix} \frac{\partial \bar{\mathbf{a}}(\psi_i)}{\partial \psi_{x_i}} & \frac{\partial \bar{\mathbf{a}}(\psi_i)}{\partial \psi_{y_i}} \end{bmatrix} \quad i = 1, \dots, k, \quad (17)$$

and

$$\mathbf{Z} = [\mathbf{Z}_1 \quad \mathbf{Z}_2 \quad \dots \quad \mathbf{Z}_k], \quad (18)$$

which forms an $N \times 2k$ matrix. Here, we define

$$\mathbf{H} \triangleq \begin{bmatrix} \mathbf{Z}_{\psi^{az}}^H \mathbf{Z}_{\psi^{az}} & \mathbf{Z}_{\psi^{az}}^H \mathbf{Z}_{\psi^{el}} \\ \mathbf{Z}_{\psi^{el}}^H \mathbf{Z}_{\psi^{az}} & \mathbf{Z}_{\psi^{el}}^H \mathbf{Z}_{\psi^{el}} \end{bmatrix} \quad (19)$$

We use the subscript 2 to denote that ψ_i has two components. We define a 2×2 matrix of ones as

$$\mathbf{1}_{2 \times 2} = \begin{bmatrix} 1 & 1 \\ 1 & 1 \end{bmatrix}. \quad (20)$$

Therefore, the expression for the FIM under i.i.d. snapshots is

$$\mathbf{J} = \frac{2K}{\sigma_w^2} [\text{Re} [\mathbf{H} \odot [\mathbf{S}_f^T \otimes \mathbf{1}_{2 \times 2}]]], \quad (21)$$

where σ_w^2 , K , S_f , \otimes , and \odot denote the noise variance, the number of snapshots, the source signal powers, and the

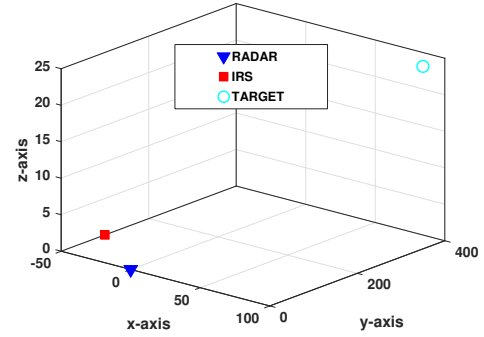


Fig. 3: Proposed Configuration in 3-Dimensional Space

Kronecker and Hadamard products, respectively. The resulting CRB matrix is given by

$$\mathbf{C}_{CR} = \mathbf{J}^{-1} \quad (22)$$

$$\mathbf{C}_{CR} = \begin{bmatrix} \mathbf{C}_{\psi^{az}, \psi^{az}} & \mathbf{C}_{\psi^{az}, \psi^{el}} \\ \mathbf{C}_{\psi^{el}, \psi^{az}} & \mathbf{C}_{\psi^{el}, \psi^{el}} \end{bmatrix} \quad (23)$$

Consequently, the variance and Root-Mean-Square Error (RMSE) for azimuth and elevation estimates are obtained as

$$\text{var}(\psi_{az}) = C_{\psi_{az}, \psi_{az}}, \text{RMSE}(\psi_{az}) = \sqrt{C_{\psi_{az}, \psi_{az}}} \quad (24)$$

$$\text{var}(\psi_{el}) = C_{\psi_{el}, \psi_{el}}, \text{RMSE}(\psi_{el}) = \sqrt{C_{\psi_{el}, \psi_{el}}} \quad (25)$$

V. RESULTS

We evaluate the performance of the proposed radar-IRS system using a simulated 24 GHz sensing configuration. The radar transmitter (Tx) and receiver (Rx) are co-located at the origin, $(0, 0, 0)$ m, and operate at a carrier frequency of $f_0 = 24$ GHz, corresponding to a wavelength of $\lambda = 0.0125$ m. The receive aperture is a uniform linear array (ULA) composed of $M_R = 50$ elements placed along the x -axis, with half-wavelength spacing $d_{\text{radar}} = \lambda/2 = 6.25$ mm. Hence, the m -th receive sensor is located at $((m-1)d_{\text{radar}}, 0, 0)$.

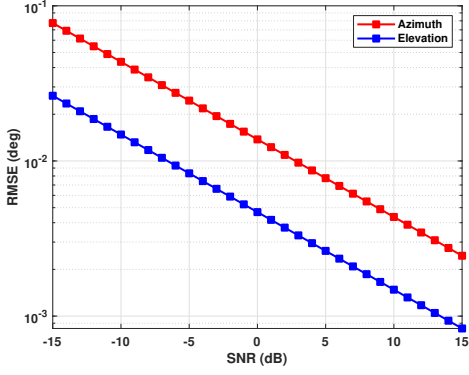


Fig. 4: RMSE vs SNR behavior of IRS-static Radar

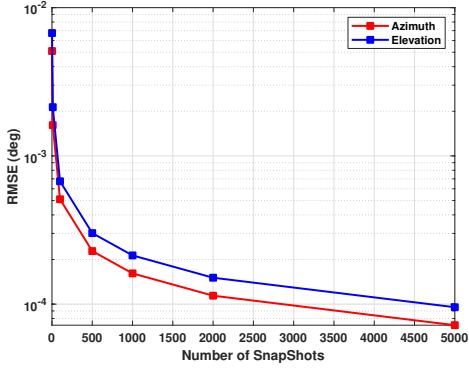


Fig. 5: RMSE vs number of Snapshots

A single IRS panel is positioned at $(-50, 100, 0)$ m as shown in Fig. 3 and realized as a 20×18 rectangular grid of reflecting elements, resulting in $L_{\text{total}} = 360$ controllable units. The IRS elements are arranged in the y - z plane with half-wavelength spacing along both axes, i.e., $d_{\text{irs},y} = d_{\text{irs},z} = \lambda/2$. In addition to geometric placement, the complex reflection weights of the IRS are designed to jointly align the incident radar signal from the target direction assumed to be at $[5, 35, 18]$ with the desired outgoing look-up direction toward the radar receiver. All propagation is modelled under free-space conditions with wave speed $c = 3 \times 10^8$ m/s, and half-wavelength sampling is employed across all arrays to avoid grating lobes and preserve directional integrity at 24 GHz.

Fig. 4 shows that azimuth and elevation angle RMSEs (on a logarithmic scale) decrease steadily as SNR increases from -15 dB to 15 dB, confirming improved estimation accuracy with stronger signals. The azimuth and elevation curves remain separated across all SNRs, indicating systematically better accuracy in one angular dimension due to the radar-IRS geometry and its effective aperture and directional gain. At moderate-to-high SNRs, the RMSE drops sharply, revealing that reliable sub-degree angle estimation is achievable once the SNR surpasses a mid-range threshold.

The Figure 5 analyzes how azimuth and elevation RMSE vary with the number of snapshots (on a logarithmic scale). Both errors decrease as snapshots increase from hundreds to thousands, with the largest RMSE in the low-snapshot regime and diminishing improvements thereafter as the covariance

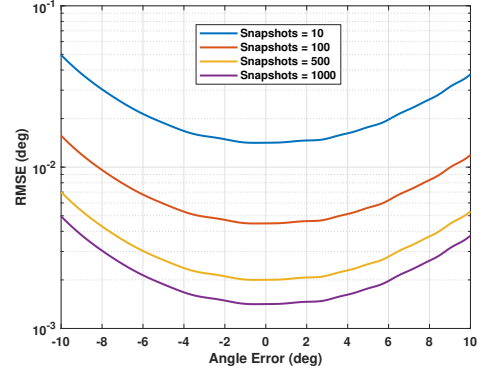


Fig. 6: RMSE vs Deviation in Azimuth of Target from the IRS Target lookup direction

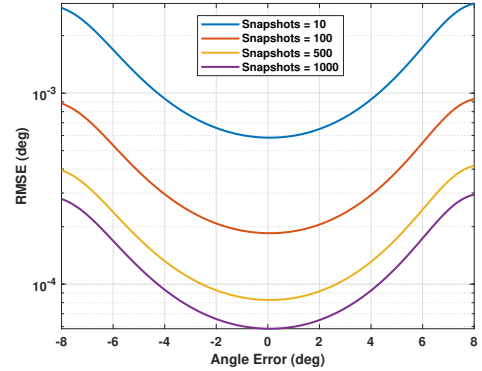


Fig. 7: RMSE vs Deviation in Elevation of Target from the IRS Target lookup direction

estimate stabilizes. Throughout, elevation and azimuth RMSE curves remain separated, reflecting the anisotropic array-IRS geometry that inherently favors one angular dimension. Overall, the results show that structural aspects of the sensing configuration drive performance disparities, and that increasing snapshots significantly enhances angle estimation reliability, especially at moderate SNR.

In our experiment, we have now set the IRS look-up direction and the nominal target position to $[5, 35, 18]$. Controlled signed perturbations were applied to the target's azimuth and elevation angles separately within $\pm 10^\circ$, and the resulting changes in the Cramér-Rao lower bound (CRLB) were analyzed as the target deviated from the look-up direction, as shown in Figures 6 and 7. The RMSE increased with mismatch magnitude, indicating reduced Fisher information due to misalignment between the reflected field and the beam. The symmetry around zero mismatch suggests that equal under- and over-steering have similar effects on accuracy. Increasing the number of snapshots from 10 to 1000 improved covariance estimation, lowered the CRLB, and reduced the RMSE across the entire error range.

Figure 8 shows how azimuth and elevation RMSE depend on IRS elements, using a logarithmic scale. As N_{IRS} increases from 0 to 100, both RMSE values decline steadily, highlighting the impact of aperture gain in IRS-assisted sensing. Larger IRS panels enhance array gain and phase shaping, boosting

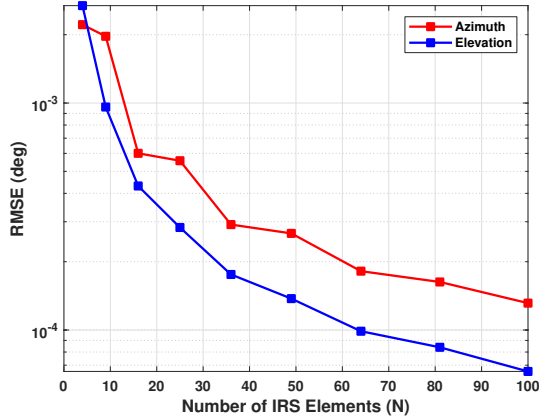


Fig. 8: RMSE vs Number of IRS elements

reflected signals and angular resolution. RMSE reduction is more significant between $N = 0$ and 40, then flattens, indicating diminishing returns as aperture grows. Elevation RMSE always exceeds azimuth RMSE, reflecting anisotropy from the radar-IRS setup and array geometry. Overall, increasing IRS elements benefits the low- to mid-range aperture, but optimising design balances hardware costs and performance at larger sizes.

VI. CONCLUSION

This study examined NLoS sensing and stealth-target detection using an IRS-based configuration termed ‘IRS-static radar’. Unlike traditional IRS-assisted radar that requires a significant four-hop path, this setup uses signals scattered by the target, received at the IRS and sent back to the radar, mimicking bi-static sensing but with a mono-static radar front end. This method offers a practical way to detect low-observable targets. A systematic signal model for the IRS-static radar was developed and reformulated for target parameter estimation. Using this model, we derived closed-form Fisher Information Matrix (FIM) and Cramér-Rao Lower Bounds (CRLB) for target angle estimation, making the analysis more straightforward.

Numerical results demonstrated that estimation accuracy improves with higher SNR and more snapshots. The system’s sensitivity to IRS pointing and beamforming was observed, with performance decreasing as the target moves away from the steering direction. Increasing IRS elements improved bounds due to better passive beamforming and resolution. Elevation estimates were more accurate than azimuth estimates due to the array geometry, guiding the optimization of IRS size and steering for reliable parameter estimation in challenging environments. Overall, the IRS-static radar enhances sensing capabilities and addresses limitations of current IRS-assisted systems. Future work includes optimizing IRS placement and phase profiles, and validating them experimentally with measured channels and hardware prototypes.

In addition to the work carried out, we will develop an estimation algorithm and evaluate the performance of various estimation algorithms for the configuration and signal model discussed.

REFERENCES

- [1] Z. Wu, J. Song, Z. Wang, and Q. Wang, “Passive radar multi-target detection experimental study at sea,” in *2024 9th International Symposium on Computer and Information Processing Technology (ISCIPT)*, 2024, pp. 414–418.
- [2] D. Wang, Z. Liu, S. Dou, J. Dai, Y. Lu, and Q. Liu, “Active and passive radar cooperative target tracking method assisted by doppler information,” in *2024 IEEE International Conference on Signal, Information and Data Processing (ICSIDP)*, 2024, pp. 1–6.
- [3] Y. Zhou, W. Zhu, Y. He, and Y. Li, “Isar image-based spatial target recognition,” in *2023 IEEE 3rd International Conference on Information Technology, Big Data and Artificial Intelligence (ICIBA)*, vol. 3, 2023, pp. 613–616.
- [4] C. Zeng, Y. Liang, and H. Li, “Joint active and passive beamforming for nlos target detection in ris-assisted mono-static radar,” in *2024 58th Asilomar Conference on Signals, Systems, and Computers*, 2024, pp. 1562–1566.
- [5] Y. Zheng, B. Zheng, Q. Wu, J. Tang, Y. Zeng, and R. Zhang, “Intelligent reflecting surface-enhanced radar detection with beam broadening,” *IEEE Communications Letters*, vol. 29, no. 11, pp. 2711–2715, 2025.
- [6] H. Zhang and J. Zheng, “Irs-assisted secure radar communication systems with malicious target,” *IEEE Transactions on Vehicular Technology*, vol. 73, no. 1, pp. 591–604, 2024.
- [7] Q. Deng, Z. Jiang, M. Huang, W. Sun, and Q. Li, “Joint beamforming and reflection design for irs-aided co-existing radar and communication,” *Electronics Letters*, vol. 61, no. 1, p. e70140, 2025.
- [8] Z. Esmailbeig, K. V. Mishra, A. Eamaz, and M. Soltanalian, “Cramér-rao lower bound optimization for hidden moving target sensing via multi-irs-aided radar,” *IEEE Signal Processing Letters*, vol. 29, pp. 2422–2426, 2022.
- [9] J. Wang, J. Fang, H. Li, and C. Masouros, “Crb optimization for intelligent reflecting surface-assisted nlos wireless sensing,” *IEEE Transactions on Signal Processing*, vol. 73, pp. 3994–4010, 2025.
- [10] B. Wang, H. Li, S. Shen, Z. Cheng, and B. Clerckx, “A dual-function radar-communication system empowered by beyond diagonal reconfigurable intelligent surface,” *IEEE Transactions on Communications*, vol. 73, no. 3, pp. 1501–1516, 2025.
- [11] C. L. Teo, “Bistatic radar system analysis and software development,” Ph.D. dissertation, Naval Postgraduate School, Monterey, Calif., 2003.
- [12] A. Zaibashi, “A unified framework for multistatic passive radar target detection under uncalibrated receivers,” *IEEE Transactions on Signal Processing*, vol. 69, pp. 695–708, 2021.
- [13] H. D. Griffiths, “Bistatic and multistatic radar,” 2004. [Online]. Available: <https://api.semanticscholar.org/CorpusID:11689105>
- [14] L. Zhang and K. Bialkowski, “Cartesian space localisation and tracking using multi-static passive radar,” in *Proc. 2025 IEEE Radar Conference (RadarConf25)*, Krakow, Poland, 2025, pp. 1188–1192.
- [15] A. Asif and S. Kandeepan, “Cooperative fusion based passive multistatic radar detection,” *Sensors*, vol. 21, no. 9, p. Article 3209, 2021. [Online]. Available: <https://www.mdpi.com/1424-8220/21/9/3209>
- [16] T. Wang and T. Huang, “Passive radar based uav detection using opportunistic rf illumination,” in *Proc. 2019 IEEE International Conference on Industrial Internet (ICII)*, Orlando, FL, USA, 2019, pp. 6–11.
- [17] J. K. A. Henry and R. M. Narayanan, “Single-receiver target detection and localization of space objects,” in *Proc. 2025 IEEE Space, Aerospace and Defence Conference (SPACE)*, Bangalore, India, 2025, pp. 1–4.
- [18] F. Colone, F. Costa, Y. Gao, C. Hao, L. Yan, G. Manara, and D. Orlando, “Ris-aided radar detection architectures with application to low-rsc targets,” 2026. [Online]. Available: <https://arxiv.org/abs/2601.10846>
- [19] M. A. Richards *et al.*, *Fundamentals of radar signal processing*. Mcgraw-hill New York, 2005, vol. 1.
- [20] S. Buzzi, E. Grossi, M. Lops, and L. Venturino, “Foundations of mimo radar detection aided by reconfigurable intelligent surfaces,” *IEEE Transactions on Signal Processing*, vol. 70, pp. 1749–1763, 2022.
- [21] X. Mu, L. Zhou, H. Fu, and J. Dai, “Target localization for IRS-assisted massive mimo systems,” *IEEE Sensors Journal*, vol. 23, no. 23, pp. 29 260–29 270, 2023.
- [22] T. H. L. Van *Optimum Array Processing: Part IV of Detection, Estimation, and Modulation Theory*. New York: John Wiley & Sons, 2002.